

Comparing vegetation indices from Sentinel-2 and Landsat 8 under different vegetation gradients based on a controlled grazing experiment

Qi Qin, Dawei Xu, Lulu Hou, Beibei Shen, Xiaoping Xin*

National Hulunbeier Grassland Ecosystem Observation and Research Station, Institute of Agricultural Resources and Regional Planning, Chinese Academy of Agricultural Sciences, Beijing 100081 China



ARTICLE INFO

Keywords:
Aboveground biomass
Leaf area index
Grazing intensity
Grasslands
Vegetation indices

ABSTRACT

Grasslands contribute considerably to the global carbon cycle and livestock production. However, many of the world grasslands suffer from degradation caused mainly by overgrazing. Remote sensing methods are effective tools for monitoring and estimating grassland vegetation parameters. In this study, we compared the performance of vegetation indices (VIs) obtained from two different sensors to estimate grassland vegetation parameters under different vegetation and soil conditions based on typical grassland biomass gradients formed by long-term controlled grazing experiments. Sentinel-2 and Landsat 8 were selected as data sources to estimate two vegetation parameters, fresh aboveground biomass (AGB) and leaf area index (LAI). Field-measured fresh AGB and LAI data were collected from experimental grasslands with different grazing intensities (GI) in Hulunbeier, Inner Mongolia, China in 2019. Univariate linear mixed models were established between VIs and field measurements, and grazing intensities were considered as random factors. The results confirmed that vegetation parameters (AGB and LAI) and VIs decreased with increasing GI; however, the decreasing trend was insignificant when the GI exceeded 0.69 Au/ha. VIs derived from Sentinel-2 and Landsat 8 estimated fresh AGB and LAI at 80% accuracy. Sentinel-2 derived VIs yielded higher predictive accuracy than Landsat 8 for both fresh AGB and LAI. Comparing with the other VI inversion models, the normalised difference phenology index derived from Sentinel-2 images estimated the vegetation parameters the most effectively and accurately, with a coefficient of determination (R^2) of 0.625 and relative root mean square error (RMSE%) of 18.105% for fresh AGB estimation and R^2 of 0.559 and RMSE% of 14.953% for LAI estimation.

1. Introduction

Grassland ecosystems cover more than 40% of the land surface in China and account for approximately 20% of total terrestrial productivity (Scurlock and Hall, 1998; Chapin et al., 2013; Zhang et al., 2019). Grasslands contribute to biodiversity and soil conservation and play important roles in global carbon cycling and climate regulation (Poulter et al., 2014). In northern China, where grazing is the main production method, the widely distributed temperate meadow steppe supports the livestock industry and the livelihood of millions of people by providing materials and spaces (Kawamura et al., 2005). However, serious degradation of the natural grassland has occurred due to overgrazing and a lack of monitoring and management practices (Harris, 2010). Grazing intensity (GI) is a crucial index of grazing utilisation which indicates the number of livestock per unit area in a given period. It affects the conditions of grassland and soil; furthermore, high GI leads to

low production efficiency (Kawamura et al., 2005; Xu et al., 2019). Biomass and leaf area index (LAI) are key biophysical parameters used to characterize grassland growth conditions (Baghdadi et al., 2016; Klemas, 2013; Yu et al., 2018). The aboveground biomass (AGB) represents the quality of forage and the herbivore-carrying capacity in pasture areas (Jobbágó et al., 2002; Dong et al., 2003). The LAI describes the vegetation structures and is closely related to vegetative photosynthesis and energy balance (Running, 1989; Sellers et al., 1997). Hence, monitoring and estimation of AGB and LAI are essential for evaluating grasslands and improving management methods.

Traditional approaches to estimating AGB and LAI are time-consuming, labour-intensive, and destructive to grasslands (Schellberg and Verbruggen, 2014). Remote sensing technology has been instrumental in improving land monitoring and management decisions, as it observes land surfaces with large extents and a fine time resolution (Bastiaanssen et al., 2000). Moreover, grassland vegetation can be

* Corresponding author.

E-mail address: xinxiaoping@caas.cn (X. Xin).

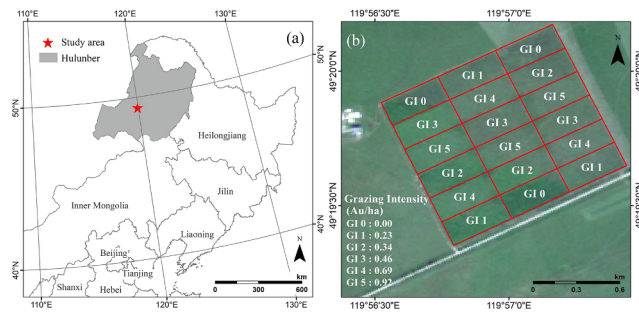


Fig. 1. (a) Location of the study area; (b) 10-m resolution true colour map of the grazing area overlaid from Sentinel-2B images with sensing date on August 1st, 2019, red = B4, green = B3, blue = B2.

monitored, quantified, and evaluated using remote sensing technology as it provides spectral, temporal, and spatial information (Wachendorf et al., 2018). Optical remote sensors, such as the Moderate Resolution Imaging Spectroradiometer (250/500 m) (John et al., 2018), SPOT satellites (10/20 m) (Güneralp et al., 2014), Landsat satellites (30 m) (Zhang et al., 2018), Sentinel satellites (10/20 m) (Xie et al., 2019), and WorldView satellites (1.24 m) (Bao et al., 2019) have provided primary data sources for grassland vegetation estimation owing to their multi-spectral, multi-temporal, and multi-spatial resolution. Vegetation indices (VIs) inversion models have been widely used in AGB and LAI estimations (Misra et al., 2020). Traditional VIs using a combination of red, blue, and near-infrared bands (Fan et al., 2009; Jin et al., 2014), and more recently, short-wave infrared bands (Li and Guo, 2018) and red-edge bands (Delegido et al., 2011) have been implemented in VIs to improve the capability of VIs to explain vegetation parameters.

The majority of studies on the estimation of grassland vegetation from remote sensing data are based on statistical models that use spectral data or VIs combined with field measurements in a regression, such as linear regression (Broge and Leblanc, 2001), multiple linear regression (Guerini Filho et al., 2020), or partial least squares regression (Cho et al., 2007; Ali et al., 2014; Obermeier et al., 2019). Moreover, machine learning and geostatistical prediction methods, such as support machine vector (Xie et al., 2009), random forest (Zhu and Liu, 2015; Ge et al., 2018), ordinary kriging (Li et al., 2016a), and regression kriging (Hooten, 2007) have been developed to maximise the use of spectral information and minimise the uncertainty of estimation. These approaches have been implemented in different grass types (Guerini Filho et al., 2020), different vegetation types (Shoko and Mutanga, 2017), and under different land use management (Griffiths et al., 2020) at regional and global scales (Otgonbayar et al., 2019; Cisneros et al., 2020). However, the VI inversion models could be untransferable to different regions because the empirical model obtained in particular regions cannot represent different vegetation characteristics (Xu et al., 2019; Li et al., 2016b). Under the simulation of different grassland vegetation and background conditions, comparison of remote sensing models is valuable for the future selection of appropriate data sources and VI inversion models.

The objective of this study is to compare the performance of VIs from different sensors in estimating fresh AGB and LAI under different grassland vegetation gradients. Based on a long-term controlled grazing experiment, the study area involved different grassland vegetation conditions and biomass gradients, which represent the majority of the grazing lands in the northern meadow steppe in China (Yan et al., 2015; 2016). The relationships between vegetation parameters and VIs under different grazing levels are discussed. Estimation models of fresh AGB and LAI by VIs were established under different grassland vegetation gradients. Linear mixed models were used to map VIs to vegetation parameters, and GI was considered as the random factor. The aim of this study is to present the comparison of remote sensing models, with the hope to make a valuable contribution to the selection of appropriate

data sources and VI inversion models in future research and applications.

2. Materials and methodology

2.1. Study area

The study area is located in Xieertala Farm, Hulunbeier, Inner Mongolia, China (Fig. 1). The controlled grazing experiment was conducted in a 90-ha experimental natural grassland area of the Xieertala Farm in the grazing season from June to October 2009–2019. The annual mean temperature of the study area was 0.69 °C, and annual precipitation was 330.2 mm. During the grazing season, the daily mean temperature of the study area was 14.5 °C and the total precipitation was 305.2 mm. The dominant species of the study area are native perennials bunchgrasses, such as *L. chinensis*, *Scutellaria baicalensis*, *Carex pediformis*, *Galium verum*, *Bupleurum scorzonerifolium*, and *Filifolium sibiricum* (Yan et al., 2015). The grassland was divided into three fields and each field included six grazing intensity (GI): 0.00 (GI 0), 0.23 (GI 1), 0.34 (GI 2), 0.46 (GI 3), 0.69 (GI 4), 0.92 (GI 5) animal units, Au/ha (1 Au = a 500 kg adult cattle). Eighteen 5-ha paddocks were fenced, and 90 ha of total grassland area was used for the experiment. 0, 2, 3, 4, 6, and 8 heads of young cows were assigned to six paddocks to represent the six GI gradients, respectively. Each cow weighed 250–300 kg and they were kept in the paddock throughout the grazing season from June–October. The long-term controlled grazing experiment has led to significant changes in vegetation and soil conditions among different GIs (Yan et al., 2015; Yan et al., 2016).

2.2. Field measurements

Fresh AGB is defined as the weight of the aboveground live mass per unit area. LAI is defined as the one-sided green leaf area per unit ground surface area (Watson and Marion, 1953; Chen and Black, 1992). A 0.5 m × 0.5 m quadrat was used in field sampling. The fresh AGB was collected during the grazing season of 2019. The first sampling occurred from July 23 to 27 and the second sampling occurred from August 18 to 29. Standing green plants were cut from the ground within each quadrat and weighed to determine the fresh AGB. Eight quadrats were randomly selected from each paddock, and the fresh AGB samples were collected from 144 quadrats. Owing to the loss of GPS data of 2 quadrats, 142 of the 144 quadrats were used for the fresh AGB analysis. LAI was measured from August 25 to August 27, 2019. Five quadrats were randomly selected from each paddock, and the LAI was measured in a total of 90 quadrats, using a LAI-2200C plant canopy analyser (Li-Cor, Lincoln, Nebraska, USA). Three measurements were taken within each quadrat to obtain a single LAI value. The coordinates of each quadrat were recorded using a hand-held GPS device with 2-m accuracy.

2.3. Satellite images and pre-processing

In this study, Sentinel-2A/B Multi-spectral Instrument (MSI) and Landsat 8 Operational Land Imager (OLI) data were used. Sentinel-2A, launched in June 2015, and Sentinel-2B, launched in March 2017, occupy the same orbit separated by 180°, with a 2-d revisiting period and a transit time of $11:00 \pm 5$ min (Beijing time, the same thereafter) in the study area. Both two identical Sentinel-2 satellites carry the MSI instrument, which contains 13 spectral bands ranging from visible near infrared (VNIR) to shortwave infrared (SWIR) at 10-m, 20-m, and 60-m spatial resolutions. Landsat 8 launched in February 2013 and overpasses the study area at approximately 10:40, with a 15-d revisiting period. Landsat 8 OLI surface reflectance products have eight spectral bands covering VNIR to SWIR at a 30-m spatial resolution and a 15-m resolution panchromatic band. Sentinel-2A/B MSI level-1C products with sensing dates on July 27, July 29, August 31, and September 2, 2019 and Landsat 8 OLI surface reflectance products with sensing dates on July

Table 1

Sensor spectral and spatial characteristics.

Sentinel-2A/B MSI		Landsat 8 OLI		
Band	Wavelength (nm)	Spatial resolution (m)	Band	Wavelength (nm)
B2 (blue)	458–522	10	B2 (blue)	420–512
B3 (green)	543–577	10	B3 (green)	533–590
B4 (red)	650–679	10	B4 (red)	636–673
B8 (NIR)	726–938	10	B5 (NIR)	851–879
B11 (SWIR1)	1566–1655	20	B6 (SWIR1)	1566–1651
B12 (SWIR2)	2101–2280	20	B7 (SWIR2)	2107–2294

Only bands analysed in this study are included.

Table 2

Vegetation indices (VIs) used in the study.

Index	Name	Formula	Reference
EVI	Enhanced vegetation index	$2.5 \times \frac{NIR - RED}{NIR + 6 \times RED - 7.5 \times BLUE + 1}$	(Huete et al., 1997)
NDPI	Normalized difference phenology index	$\frac{NIR + 6 \times RED - 7.5 \times BLUE + 1}{NIR + (0.74 \times RED + 0.26 \times SWIR1)}$	(Wang et al., 2017)
NDVI	Normalized difference vegetation index	$\frac{NIR - RED}{NIR + RED}$	(Rouse et al., 1973)
SAVI	Soil adjusted vegetation index	$1.5 \times \frac{NIR - RED}{NIR + RED + 0.5}$	(Huete, 1988)
NDWI	Normalized difference water index	$\frac{NIR - SWIR1}{NIR + SWIR1}$	(Gao, 1996)
NDTI	Normalized difference tillage index	$\frac{SWIR1 - SWIR2}{SWIR1 + SWIR2}$	(Van Deventer et al., 1997)

16, August 1, and September 2, 2019 were used in this study. Sentinel-2A/B MSI level-1C products were downloaded from the Copernicus Open Access Hub (<https://scihub.copernicus.eu>). Landsat 8 OLI surface reflectance products were downloaded from NASA Earthdata (<https://earthdata.nasa.gov>). The characteristics of the Sentinel-2A/B MSI and Landsat 8 OLI are listed in Table 1. Both Sentinel-2A/B MSI level-1C and Landsat 8 OLI level-1 images were geometrically corrected. Landsat 8 OLI surface reflectance images were atmospherically corrected, and clouds, shadows, water, and snow were masked. Atmospheric correction for Sentinel-2A/B images was performed using the Sen2cor 02.08.00 tool. All Sentinel-2A/B 10-m resolution bands were resampled to a 20-m resolution using the nearest neighbour resampling tool in the Sentinel Application Platform (SNAP) 7.0.0.

Six VIs were used in this study, which were calculated based on the reflectance of the top canopy. The names and formulas of six VIs are given in Table 2, and the bands used in the calculation are listed in Table 1. The normalised difference vegetation index (NDVI) and enhanced vegetation index (EVI) are the most widely used VIs for vegetation monitoring, estimation, and health detection (Ding et al., 2019; Li et al., 2017). The normalised difference phenology index (NDPI) was designed to remove the impact of snow and bare soil background on vegetation by replacing the red band with the “RED + SWIR” (Wang et al., 2017; Chen et al., 2019). Moreover, it could reduce the VI model saturation to vegetation biomass, increasing the precision of the estimated models in both low- and high-biomass areas (Djamai et al., 2019). The soil adjusted vegetation index (SAVI) was developed to minimise the influence of spectral VIs involving red and near-infrared (NIR) wavelengths (Jin et al., 2014). The normalised difference water index (NDWI) is used to monitor changes in the water content of leaves using NIR and short-wave infrared (SWIR) wavelengths (Gao, 1996; Otgonbayar et al., 2019). The normalised difference tillage index (NDTI) is a short-wave infrared index, which is capable of distinguishing non-photosynthetic vegetation biomass from green vegetation biomass (Li

and Guo, 2018; Dai et al., 2018).

2.4. Data analysis

Data were analysed using the statistical software package R 3.6.3. Preliminary data analysis was performed prior to modelling. Data normality was tested using the Shapiro-Wilk test, and non-normally distributed data were transferred to the normal distribution using the Box-Cox transformation. Linear Pearson correlation analysis and analysis of variance (ANOVA) were conducted. All tests were evaluated at a 95% confidence level.

2.4.1. Linear mixed model

Owing to the impact of grazing on vegetation canopy structure and topsoil (Yan et al., 2015), linear mixed models were used to estimate fresh AGB and LAI values. Linear mixed models are an improvement of simple linear models as they incorporate fixed factors and random factors and are particularly used for data with a hierarchical structure (Kiviet, 2009). Linear mixed models can explore the differences between the effects within and between groups. A linear mixed model can be represented as:

$$Y = \beta X + \mu Z + \varepsilon \quad (1)$$

where Y is the outcome variable; X is the fixed factor; Z is the random factor; β and μ are coefficients; and ε is the random error. In this study, linear mixed models were established using VI and field measurements. The outcome variables were the field-measured fresh AGB and LAI; the VIs and GIs were fixed and random factors, respectively. For all models, the predicted and residual values were calculated to satisfy the assumptions of normality and homoscedasticity. The bootstrapping approach was implemented in modelling for added robustness, and 500 iterations were performed for each model.

2.4.2. Model validation

The coefficient of determination (R^2) was calculated for models with random factors to assess the impact of random effects on models (Nakagawa et al., 2017). In addition, the R^2 , root mean square error (RMSE), and relative RMSE (RMSE%) between the measured values and estimated values were used to evaluate the modelling results for fresh AGB and LAI predictions. The R^2 , RMSE, and RMSE% were calculated as follows:

$$R^2 = 1 - \frac{\sum_{i=1}^N (y_i - \hat{y}_i)^2}{\sum_{i=1}^N (y_i - \bar{y})^2} \quad (2)$$

$$RMSE = \sqrt{\frac{1}{N} \sum_{i=1}^N (\hat{y}_i - y_i)^2} \quad (3)$$

$$RMSE\% = \frac{RMSE}{\bar{y}} \times 100\% \quad (4)$$

where y_i is the field-measured value; \hat{y}_i is the estimated value; and \bar{y}

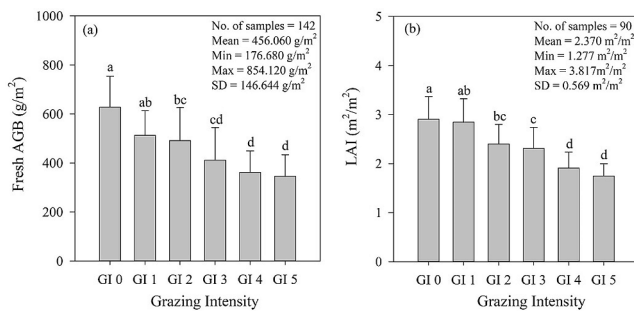


Fig. 2. Mean and standard deviation (error bars) of (a) fresh AGB and (b) LAI under different GIs. Lowercase letters indicate the multiple comparisons of LAI and fresh AGB among grazing intensities.

Table 3
Correlation coefficients between VIs and fresh AGB, LAI, and GI.

Correlation Coefficient	Fresh AGB		LAI		GI	
	MSI-	OLI-	MSI-	OLI-	MSI-	OLI-
EVI	0.610*	0.511*	0.649*	0.552*	-0.321*	-0.218*
NDPI	0.763*	0.728*	0.730*	0.690*	-0.676*	-0.499*
NDVI	0.748*	0.723*	0.707*	0.698*	-0.557*	-0.569*
SAVI	0.631*	0.559*	0.654*	0.598*	-0.347*	-0.294*
NDWI	0.525*	0.725*	0.726*	0.680*	-0.613*	-0.566*
NDTI	0.393*	0.617*	0.700*	0.697*	-0.583*	-0.549*
GI	-0.628*		-0.732*		—	

* indicates p-values < 0.05.

is the mean of the field-measured values. The establishment and evaluation of models were accomplished by the statistical packages “lme4”, “boot”, “merTools”, “Metrics”, and “MuMIn” in R 3.6.3. To implement the linear mixed models of VIs, fresh AGB and LAI predictions were mapped for the study area. The most accurately performing linear mixed model was used to calculate the LAI and fresh AGB maps.

3. Results

3.1. Relationships between VIs and vegetation parameters

The descriptive statistics of field measurements was given in Fig. 2 and the mean and standard deviation values of fresh AGB and LAI for all GIs are shown. A total of 142 fresh AGB and 90 LAI values were used in the data analysis. It is notable that the mean AGB and LAI decreased with an increasing GI. Both the fresh AGB and LAI were significantly different among different GIs, except for the high GI (GI 4 [0.69 Au/ha] and GI 5 [0.92 Au/ha]). Under moderate GIs (GI 2 and GI 3), the fresh AGB and LAI were more dispersed with higher standard deviations.

Table 4
Results of univariate linear mixed models (of 500 bootstrapped iterations) for fresh AGB and LAI predictions using MSI- and OLI-derived VIs.

		Coefficient	MSI - Intercept	R ²	Coefficient	OLI - Intercept	R ²
Fresh AGB	EVI	1358.357*	-173.713*	0.618	1054.830*	-37.279	0.591
	NDVI	1968.084*	-962.751*	0.603	1712.605*	-801.057*	0.537
	NDPI	1529.306*	-313.750*	0.625	1083.042*	-78.445*	0.601
	SAVI	1851.523*	-331.878*	0.605	1347.894*	-145.065*	0.584
	NDWI	514.912*	271.406*	0.407	935.797*	6.270	0.575
	NDTI	-264.758	527.234*	0.506	4219.383*	-876.040*	0.455
LAI	EVI	7.735*	-1.592	0.519	4.477	0.245	0.517
	NDVI	13.572*	-7.721*	0.547	11.991*	-6.742*	0.498
	NDPI	10.001*	-3.129*	0.559	9.245*	-3.011*	0.534
	SAVI	10.176*	-2.331*	0.516	6.605	-0.651	0.511
	NDWI	6.563*	-0.607	0.523	6.666*	-1.080*	0.512
	NDTI	17.270*	-2.838*	0.513	17.200*	-3.296*	0.505

* indicates p-values < 0.05 (95% CI). R² values are the means of 500 iterations.

Pearson's correlation analysis was used to quantify the relationships among the variables. The correlation coefficients are presented in Table 3. All VIs were significantly correlated with fresh AGB, LAI, and GI ($p < 0.05$). Strong positive relationships between VIs and field measurements were observed, except for MSI-derived NDTI. Both fresh AGB and LAI had strong negative correlations with GI. The MSI-derived VI showed stronger relationships with field measurements and GIs than the OLI-derived VI, except for NDWI and NDTI. The highest correlation coefficient between VI and fresh AGB was 0.763, which was the MSI-derived NDPI, followed by the MSI-NDVI and OLI-NDTI. The MSI-derived NDPI was notable because of its high correlations with both the fresh AGB and LAI. Compared with the fresh AGB, the LAI had a stronger relationship with VIs. The MSI-NDWI had the strongest correlation with the LAI, followed by the MSI-NDPI. All the VIs had negative relationships with GI. NDWI and NDTI were strongly correlated to GI, and EVI and SAVI had weak correlations with GI.

3.2. Inversion models and validation

Univariate linear mixed models were established between the VI and field measurements using the bootstrapping method. Table 4 shows the results of all the estimating models, and the mean R² of 500 iterations. Validation of the models against the field measurements is shown in Fig. 3 and Fig. 4, along with the mean RMSE and RMSE% of 500 iterations. For the estimation of fresh AGB, the MSI-derived NDPI models performed the most accurately among all the VI models, with the highest R² (0.625). The MSI-EVI model performed well (R² = 0.618), followed by the MSI-SAVI model (R² = 0.605). The MSI-NDWI model fitted the fresh AGB with the least accuracy (R² = 0.407). For the OLI-VI models, the OLI-NDPI model had the highest R² value (0.601), followed by the OLI-EVI (R² = 0.591) and OLI-SAVI (R² = 0.584) models. Similarly, linear mixed models were established between the VIs and LAI. The coefficients of the OLI-EVI and OLI-SAVI models were not significant at the 95% confidence level. The MSI-NDPI model had the highest R² (0.559), followed by the MSI-NDVI (R² = 0.547) and the OLI-NDPI (R² = 0.534) models. The OLI-NDVI had the lowest accuracy (R² = 0.498).

To validate the estimation models, the estimated mean values, RMSE, and RMSE% of 500 iterations were calculated. The relationships between the predictions and measurements are plotted in Fig. 3 and Fig. 4. In Fig. 3, model saturation and underestimation can be observed in most of the fresh AGB models, except for in the MSI-NDPI model (Fig. 3[c]), which also had the lowest RMSE 82.542 g/m² and RMSE% 18.105%. The MSI-NDVI model had the second lowest RMSE and RMSE% values (82.686 g/m² and 18.137%, respectively), followed by the OLI-NDPI model (84.963 g/m² and 18.636%, respectively), and the MSI-SAVI model (85.069 g/m² and 18.661%, respectively). The MSI-NDWI model had the lowest accuracy, with an RMSE of 107.835 g/m² and an RMSE% of 23.652%. The VI models estimated fresh AGB at approximately 80% accuracy, except for the NDWI and NDTI models, whereas

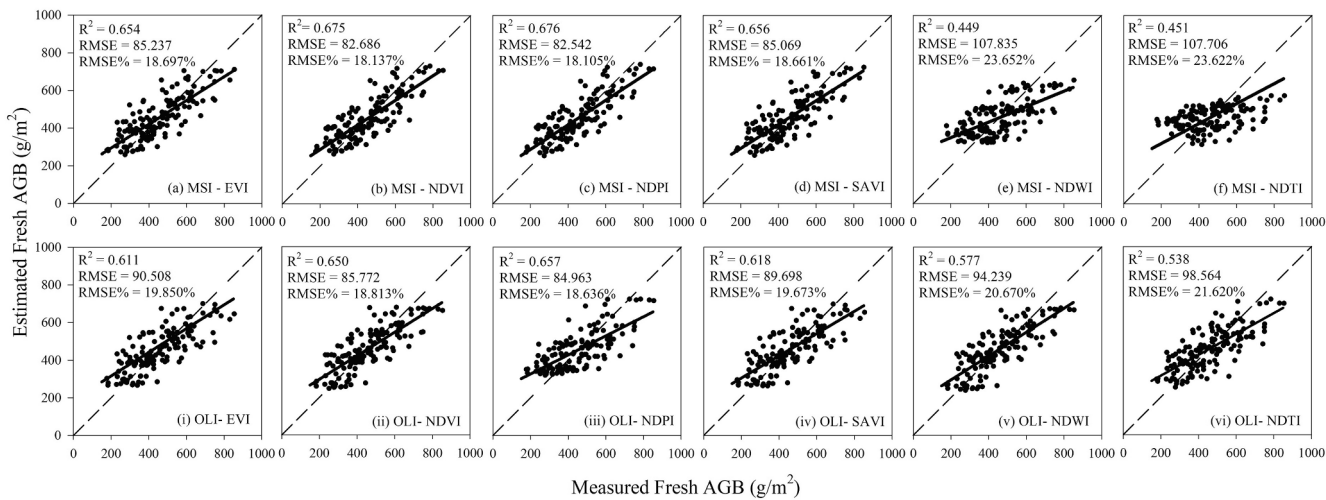


Fig. 3. Relationships between the measured fresh AGB and estimated fresh AGB: (a-f) MSI-VI; (i-vi) OLI-VI, including R^2 , RMSE, and RMSE% (means of 500 iterations).

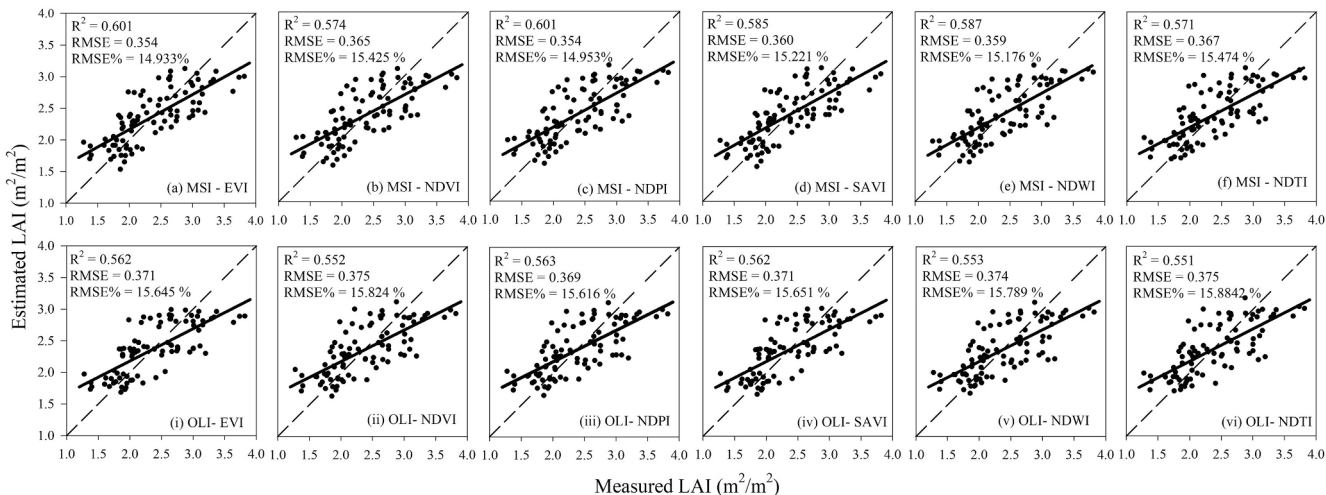


Fig. 4. Relationships between the measured LAI and estimated LAI: (a-f) MSI-VI; (i-vi) OLI-VI, including R^2 , RMSE, and RMSE% (means of 500 iterations).

the MSI models were more accurate than the OLI models in general. Similar to the fresh AGB-estimated models, the LAI models also showed saturation and underestimation. The most accurate model for LAI was the MSI-EVI model ($0.354 \text{ m}^2/\text{m}^2$ and 14.933%, respectively) followed by the MSI-NDPI model ($0.354 \text{ m}^2/\text{m}^2$ and 14.953%, respectively) and the MSI-NDWI model ($0.359 \text{ m}^2/\text{m}^2$ and 15.176%, respectively). The most accurate model of OLI-VIs was the OLI-NDPI model, with an RMSE of $0.369 \text{ m}^2/\text{m}^2$ and RMSE% = 15.616%, and the least accurate model was the OLI-NDTI model ($0.375 \text{ m}^2/\text{m}^2$ and RMSE% = 15.842%, respectively). The accuracy of the LAI models was approximately 85%, which was higher than that of the fresh AGB models. However, the saturation and underestimation of LAI models were more significant.

3.3. Fresh AGB and LAI simulations

Comparing the inversion models and validation results, the MSI-NDPI linear mixed model showed the highest R^2 and lowest RMSE% in the fresh AGB and LAI estimations. Thus, the spatial distribution maps (Fig. 5) of fresh AGB and LAI in the study area were simulated using the MSI-NDPI linear mixed model. Four Sentinel-2 images (July 27, July 29, August 31, and September 2, 2019) were used for fresh AGB and LAI mapping. As shown in the prediction maps (Fig. 5), there were visible differences among GIs in all images, especially in those from July 27 and

July 29, 2019. Heavily grazed areas were detected, while moderate and low grazing intensity levels in the predicted maps were difficult to identify. It is notable that after August 31, 2019, a burnt area appeared in the study area, while the GI gradients remained clear within both burnt and unburnt areas. Fig. 6 shows that the estimated fresh AGB and LAI changed over time under different GIs. Decreasing trends were observed over time, and the fresh AGB declined more significantly than the LAI. Regarding the estimated fresh AGB, there was no significant decreasing trend during the first 2 days, after which it decreased rapidly, except in the light grazing areas (GI 0). The fresh AGB of moderate grazing areas (GI 3) declined rapidly. In contrast, the estimated LAI values did not change significantly during the grazing season.

4. Discussion

We analysed the relationships among VIs, grazing intensities, and vegetation parameters; fitted the VI to the field measured LAI and fresh AGB using the bootstrapped linear mixed model; evaluated the performance of each VI model; and mapped the predicted fresh AGB and LAI of the 2019 grazing season in the study area. Overall, the selected VIs in this study were significantly positively correlated with the fresh AGB and LAI. The field measured fresh AGB and LAI showed negative relationships with the GI, and these relationships were more significant at

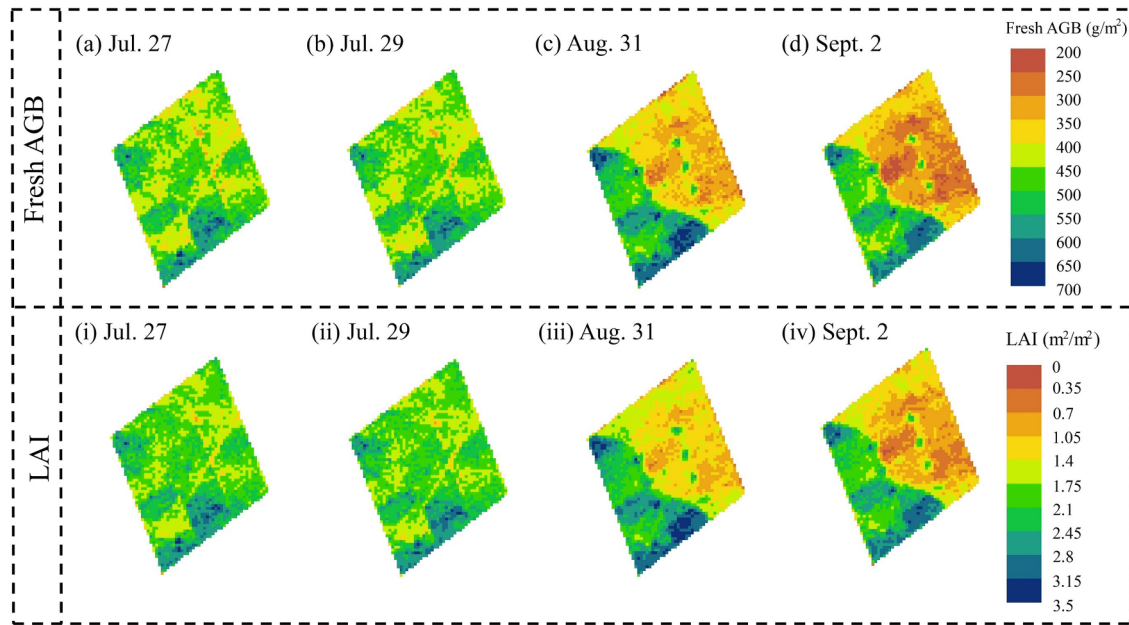


Fig. 5. Estimated fresh AGB and LAI maps of the study area on different dates using the linear mixed models: (a–d) estimated fresh AGB; (i–iv) estimated LAI.

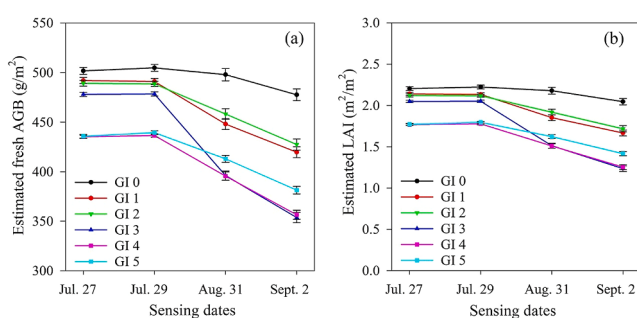


Fig. 6. Estimated (a) fresh AGB and (b) LAI changes over the grazing season under different GIs.

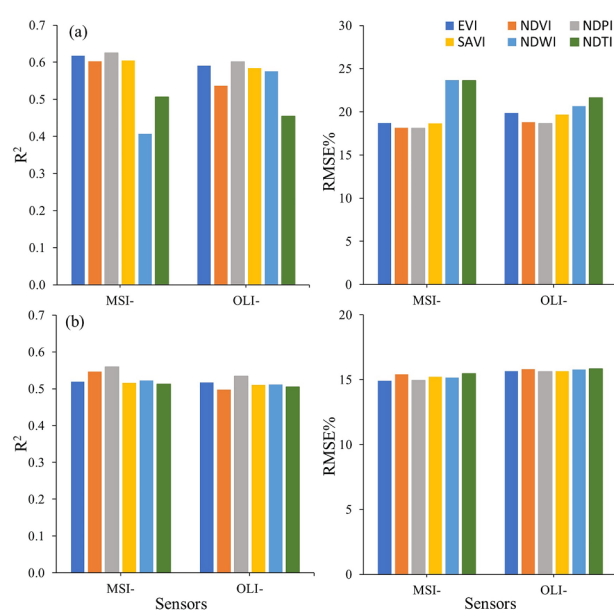


Fig. 7. Comparison of VI models for estimating fresh AGB and LAI: (a) R^2 and RMSE% of AGB models; (b) R^2 and RMSE% of LAI models.

low GI levels than at high levels.

4.1. Comparison of VI inversion models

This study compared the effectiveness of VIs obtained from different sensors to estimate vegetation parameters under different grassland biomass gradients. Univariate linear mixed models were established between VIs and field measurements, and grazing intensities were considered as random factors; 500 bootstrapped iterations were performed. By comparing the results of the models (Fig. 7), we found that the NDPI had the highest R^2 and lowest RMSE% values. Most VI models estimated vegetation parameters with an accuracy of approximately 80%. Underestimation and saturation were observed in all models except the MSI-NDPI model. The VI-LAI model was more accurate than

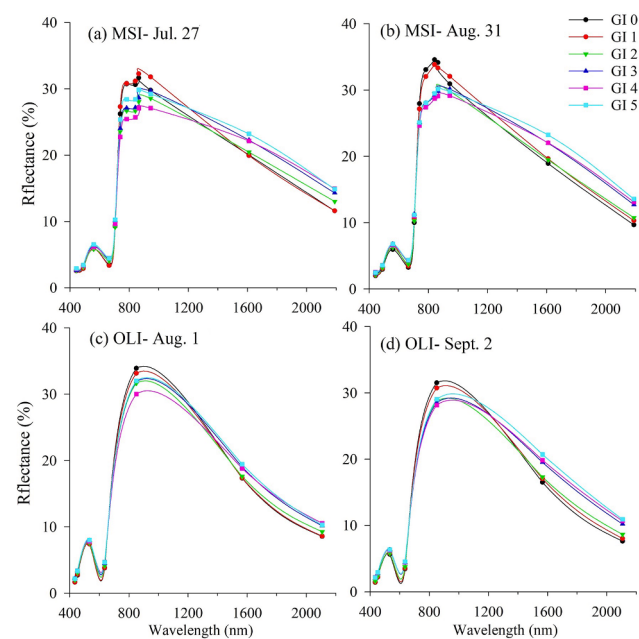


Fig. 8. Spectral reflectance curves of (a and b) Sentinel-2 and (c and d) Landsat 8 images under different grazing intensities (GIs).

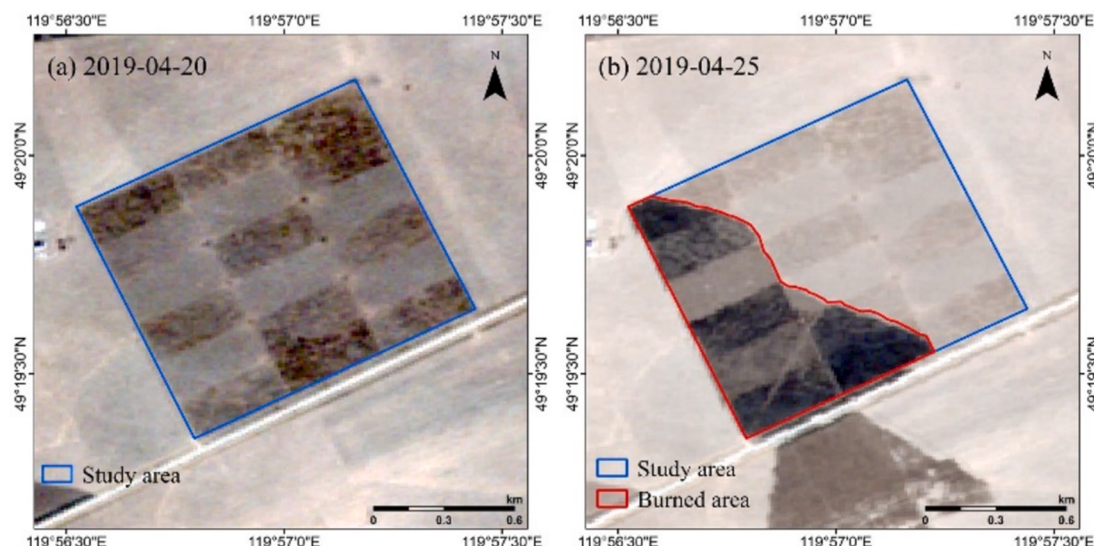


Fig. 9. Sentinel-2 10-m resolution true-colour images of study area before and after fire: (a) Study area before the fire, imaging on April 20, 2019, with the study area in blue; (b) Study area after the fire, imaging on April 25, 2019, with the burned area in red and the study area in blue.

the VI-AGB model. Comparing the two sensors, the Sentinel-2 MSI was more effective and accurate than the Landsat 8 OLI in estimating vegetation parameters, owing to the higher spatial and spectral resolutions. These results indicate the importance of selecting suitable VIs and satellite sensors for different biomass gradients.

Our study shows that NDPI was the most effective and accurate method for fresh AGB and LAI estimations. According to the Fig. 2, the fresh AGB of the study area ranged from 176.68 to 456.06 g/m² and the LAI ranged from 1.277–3.817 m²/m². The coefficient of variation of fresh AGB and LAI was 32.15% and 24.01% respectively. This indicates that both the AGB values and LAI values in the study area were seriously discrete due to the grazing gradients. From the Fig. 3[c] and Fig. 3[iii], we found that the relations between NDPI and AGB were more distinguished than other VIs. A similar pattern also showed in LAI. This means that NDPI had a wider range of applications than traditional VIs. Xu (Xu et al., 2021) proved that on the regional scale, the MODIS derived NDPI estimated AGB robustly for different sampling sizes and the NDPI-based model also had superior spatial and temporal scalability. The NDPI was designed to contrast vegetation signals from different backgrounds by suppressing the soil and alleviating atmospheric effects (Wang et al., 2017; Chen et al., 2019). Similarly, the SAVI also performed well in predicting fresh AGB and LAI because it improved the detection of vegetation by adjusting the soil background. The spectral characteristics of different underlying surfaces are the basis of remote sensing parameter inversion (Wang et al., 2017), and there were differences in spectral characteristics under different grassland biomass gradients (Fig. 8). The differences in grassland vegetation led to different spectral characteristics; Fig. 8 shows that the spectral reflectance of different vegetation biomass gradients differed most notably at wavelengths of 840 nm and 1500 nm. Furthermore, the reflectance of low GI areas (GI 0 and GI 1) decreased more significantly between the near-infrared band (840 nm) and the short-wave infrared band (1500 nm), compared with the heavy grazing areas. This was more evident in the MSI spectral reflectance curves. This variation provides a theoretical explanation for the NDPI estimation of vegetation parameters.

4.2. Impacts of fire and grazing on grassland vegetation

In previous sections, four Sentinel-2 images were used to map the spatial distributions of the estimated fresh AGB and LAI to validate the VI models. The spatial distributions of fresh AGB and LAI were capable of identifying the GI gradients of the study area, especially in overgrazed

areas. Moreover, there was an obvious burning scar on Fig. 5, whereas the AGB and LAI values of the burnt area were significantly higher than those of the unburnt area. A naturally started fire in the study area occurred on April 24, 2019, lasted about half an hour, and finally went out due to the wind direction and barriers between paddocks. Satellite images before and after the fire were given in Fig. 9. For the native perennial bunchgrasses dominant in the study area, burning removes litter and leads to annual grasses and a transient increase in native species richness and biomass within the first-year post-fire (Wedell, 2001). According to previous studies on remote sensing of wildfires and burning areas, rapid recovery of the burnt area after early spring burning will occur during the vegetation green-up period, and the burning area may remain identifiable until mid-June (Mohler and Douglas, 2010). Some studies indicate that community density, species richness, and diversity of grasslands increase within 1 year after spring burning (Pereira, 2003). This can explain why the fresh AGB and LAI of the burnt area were higher than those of the unburnt area. In this study, the remote sensing inversion models of vegetation parameters were established without separating burned and unburned areas. Instead, the study considered the grazing intensity when estimating the relations between VIs and vegetation parameters. Burning and grazing have similar effects on native species richness, cover, and composition because they both decrease non-native cover and remove accumulated litter biomass. Burning effects are temporary and burning has a greater effect on the composition of ungrazed than grazed communities (Hernández et al., 2021). Initially, burning increased the biomass of ungrazed areas. Meanwhile, these burning effects decreased with the introduction of grazing. On another hand, burning cleans litter and reduces the evenness of vegetation communities. This causes the change of underlying surfaces and thus leads to different spectral characteristics. In this context, the NDPI models still showed the best fitness for the different underlying surfaces.

5. Conclusion

In conclusion, models connecting VIs and vegetation parameters were established based on different vegetation biomass gradients. The VIs from different sensors were able to estimate vegetation parameters under different vegetation conditions. The NDPI exhibited a superior performance in estimating vegetation parameters compared to traditional VIs. Thus, in future studies, these models could be implemented at different scales. However, this study has some limitations. First, the

spectral information of satellite images and the spectral reflectance characteristics of vegetation were not fully utilised, especially for the Sentinel-2 data, which had red-edge bands that are sensitive to vegetation conditions (Vincini et al., 2014). Second, some variables were ignored in this study, such as soil moisture and temperature, landform, and grass height. Moreover, we found that the fresh AGB and LAI differed significantly between the burnt and unburnt areas after August. A possible reason may be that the burnt area had less non-photosynthetic vegetation, which affected the spectral reflectance. The detailed reasons for this will be investigated in future studies. Above all, this study has explained that monitoring and estimation of fresh AGB and LAI are essential for evaluating grassland conditions and improving management methods, so as to reduce degradation of these globally important ecosystems. This study provides new and important information that may contribute to developing in the methods used to monitor grassland vegetation with more accurate techniques.

CRediT authorship contribution statement

Qi Qin: Conceptualization, Methodology, Formal analysis, Visualization, Data curation, Writing – original draft, Writing – review & editing. **Dawei Xu:** Methodology, Validation, Investigation, Resources, Data curation. **Lulu Hou:** Methodology, Validation, Investigation, Data curation, Resources. **Beibei Shen:** Investigation, Data curation, Resources. **Xiaoping Xin:** Funding acquisition, Supervision, Project administration, Writing – review & editing.

Declaration of Competing Interest

The authors declare that they have no known competing financial interests or personal relationships that could have appeared to influence the work reported in this paper.

Acknowledgements

We are grateful to many colleagues at the Hulunber Grassland Ecosystem Observation and Research Station, Institute of Agricultural Resources and Regional Planning, Chinese Academy of Agricultural Sciences, for their assistance with field observations and sample collection.

Funding

This work was supported by the National Natural Science Foundation of China (41771205, 31971769); the National Key Research and Development Program of China (2017YFE0104500, 2021YFD1300084); the China Agriculture Research System of MOF and MARA; the Fundamental Research Funds Central Non-profit Scientific Institution (Y2019YJ13, Y2020YJ19, 1610132021016).

References

- Ali, I., Fiona, C., Stuart, G., Ned, D., 2014. Application of statistical and machine learning models for grassland yield estimation based on a hypertemporal satellite remote sensing time series. *Geoscience & Remote Sensing Symposium IEEE* 5060–5063. <https://doi.org/10.1109/IGARSS.2014.6947634>.
- Baghdadi, N., Mohammad, E.H., Mehrez, Z., 2016. Coupling SAR C-band and optical data for soil moisture and leaf area index retrieval over irrigated grasslands. *Geoscience & Remote Sensing Symposium* 3551–3554.
- Bastiaanssen, W.G.M., David, J.M., Ian, W.M., 2000. Remote sensing for irrigated agriculture: examples from research and possible applications. *Agric. Water Manag.* 46 (2), 137–155. [https://doi.org/10.1016/S0378-3774\(00\)00080-9](https://doi.org/10.1016/S0378-3774(00)00080-9).
- Broge, N.H., Leblanc, E., 2001. Comparing prediction power and stability of broadband and hyperspectral vegetation indices for estimation of green leaf area index and canopy chlorophyll density. *Remote Sens. Environ.* 76 (2), 156–172. [https://doi.org/10.1016/S0034-4257\(00\)00197-8](https://doi.org/10.1016/S0034-4257(00)00197-8).
- Bao, N., Li, W., Gu, X., Liu, Y., 2019. Biomass estimation for semiarid vegetation and mine rehabilitation using Worldview-3 and Sentinel-1 SAR imagery. *Remote Sens.* 11 (23) <https://doi.org/10.3390/rs11232855>.
- Chapin, F. S., Sala, O. E., Huber-Sannwald, E., 2013. Global biodiversity in a changing environment: scenarios for the 21st Century.
- CHEN, J.M., BLACK, T.A., 1992. Defining leaf area index for non-flat leaves. *Plant, Cell Environ.* 15 (4), 421–429.
- Chen, X., Guo, Z., Chen, J., Yang, W., Yao, Y., Zhang, Y., Cui, X., Cao, X., 2019. Replacing the red band with the red-swir band (0.74 pred+ 0.26 pswir) can reduce the sensitivity of vegetation indices to soil background. *Remote Sens.* 11 (7) <https://doi.org/10.3390/RS11070851>.
- Cho, M.A., Andrew, S., Fabio, C., Sipke, E.W., Istiak, S., 2007. Estimation of green grass/herb biomass from airborne hyperspectral imagery using spectral indices and partial least squares regression. *International Journal of Applied Earth Observation and Geoinformation* 9 (4), 414–424. <https://doi.org/10.1016/j.jag.2007.02.001>.
- Cisneros, A., Fiorio, P., Menezes, P., Pasqualotto, N., Van Wittenbergh, S., Bayma, G., Furlan Nogueira, S., 2020. Mapping productivity and essential biophysical parameters of cultivated tropical grasslands from sentinel-2 imagery. *Agronomy* 10 (5), 711. <https://doi.org/10.3390/agronomy10050711>.
- Dai, J., Dar, R., Philip, D., Douglas, S., 2018. Spectral-radiometric differentiation of non-photosynthetic vegetation and soil within Landsat and Sentinel 2 wavebands. *Remote Sensing Letters* 9 (8), 733–742. <https://doi.org/10.1080/2150704X.2018.1470697>.
- Delegido, J., Jochem, V., Luis, A., José, M., 2011. Evaluation of Sentinel-2 red-edge bands for empirical estimation of green LAI and chlorophyll content. *Sensors* 11 (7), 7063–7081. <https://doi.org/10.3390/s110707063>.
- Ding, L., Li, Z., Wang, X., Yan, X., Shen, B., Chen, B., Xin, X., 2019. Estimating grassland carbon stocks in Hulunbeier China, using Landsat8 OLI imagery and regression kriging. *Sensors* 19 (24), 5374. <https://doi.org/10.3390/s19245374>.
- Djamai, N., Richard, F., Marie, W., Heather, M., Kalifa, G., 2019. Validation of the sentinel simplified level 2 product prototype processor (SL2P) for mapping cropland biophysical variables using Sentinel-2/MSI and Landsat-8/OI data. *Remote Sens. Environ.* 225, 416–430. <https://doi.org/10.1016/j.rse.2019.03.020>.
- Dong, J., Robert, K.K., Ranga, B.M., Compton, J.T., Pekka, E.K., Jari, L., Wolfgang, B., Alexeyev, V., Malcolm, K.H., 2003. Remote sensing estimates of boreal and temperate forest woody biomass: carbon pools, sources, and sinks. *Remote Sens. Environ.* 84 (3), 393–410. [https://doi.org/10.1016/S0034-4257\(02\)00130-X](https://doi.org/10.1016/S0034-4257(02)00130-X).
- Fan, L., Gao, Y., Brück, H., Bernhofer, C., 2009. Investigating the relationship between NDVI and LAI in semi-arid grassland in Inner Mongolia using insitu measurements. *Theor. Appl. Climatol.* 95 (1–2), 151–156. <https://doi.org/10.1007/s00704-007-0369-2>.
- Gao, B.C., 1996. NDWI-a normalized difference water index for remote sensing of vegetation liquid water from space. *Remote Sens. Environ.* 58 (3), 257–266. [https://doi.org/10.1016/S0034-4257\(96\)00067-3](https://doi.org/10.1016/S0034-4257(96)00067-3).
- Ge, J., Meng, B., Liang, T., Feng, Q., Gao, J., Yang, S., Huang, X., Xie, X., 2018. Modeling alpine grassland cover based on MODIS data and support vector machine regression in the headwater region of the Huanghe river, China. *Remote Sens. Environ.* 218, 162–173. <https://doi.org/10.1016/j.rse.2018.09.019>.
- Griffiths, P., Nendel, C., Pickert, J., Hostert, P., 2020. Towards national-scale characterization of grassland use intensity from integrated Sentinel-2 and Landsat time series. *Remote Sens. Environ.* 238, 111124. <https://doi.org/10.1016/j.rse.2019.03.017>.
- Guerini Filho, M., Kuplich, T.M., Quadros, F.L.F.D., 2020. Estimating natural grassland biomass by vegetation indices using Sentinel 2 remote sensing data. *Int. J. Remote Sens.* 41 (8), 2861–2876.
- Güneralp, I., Anthony, M.F., Jarom, R., 2014. Estimation of floodplain aboveground biomass using multispectral remote sensing and nonparametric modeling. *Int. J. Appl. Earth Obs. Geoinf.* 33 (1), 119–126. <https://doi.org/10.1016/j.jag.2014.05.004>.
- Harris, R.B., 2010. Rangeland degradation on the Qinghai-Tibetan plateau: a review of the evidence of its magnitude and causes. *J. Arid Environ.* <https://doi.org/10.1016/j.jaridenv.2009.06.014>.
- Hernández, E., Shaw, E.A., Aoyama, L., Brambila, A., Niederer, C., Weiss, S.B., Hallett, L. M., 2021. Fire versus grazing as tools to restore serpentine grasslands under global change. *Restor. Ecol.* 29 (S1) <https://doi.org/10.1111/rec.v29.S110.1111/rec.13353>.
- Hooton, M.B., 2007. Statistical analysis of environmental space-time processes. *J. Am. Stat. Assoc.* 102480, 1477.
- Huete, A.R., 1988. A Soil-Adjusted Vegetation Index (SAVI). *Remote Sens. Environ.* 25 (3), 295–309. [https://doi.org/10.1016/0034-4257\(88\)90106-X](https://doi.org/10.1016/0034-4257(88)90106-X).
- Huete, A.R., Liu, H., Batchily, K., Van Leeuwen, W., 1997. A comparison of vegetation indices over a global set of tm images for EOS-MODIS. *Remote Sens. Environ.* 59 (3), 440–451. [https://doi.org/10.1016/S0034-4257\(96\)00112-5](https://doi.org/10.1016/S0034-4257(96)00112-5).
- Jin, Y., Yang, X., Qiu, J., Li, J., Gao, T., Wu, Q., Zhao, F., Ma, H., Yu, H., Xu, B., 2014. Remote sensing-based biomass estimation and its spatio-temporal variations in temperate grassland, northern China. *Remote Sensing* 6 (2), 1496–1513.
- Jobbagy, E.G., Sala, O.E., Paruelo, J.M., 2002. Patterns and controls of primary production in the Patagonian steppe: a remote sensing approach. *Ecology* 83 (2), 307. <https://doi.org/10.2307/2680015>.
- John, R., Chen, J., Vincenzo, G., Park, H., Xiao, J., Gabriela, S., Zutao, O., Shao, C., Raffaele, L., Qi, J., 2018. Grassland canopy cover and aboveground biomass in Mongolia and Inner Mongolia: spatiotemporal estimates and controlling factors. *Remote Sens. Environ.* 213, 34–48. <https://doi.org/10.1016/j.rse.2018.05.002>.
- Kawamura, K., Akiyama, T., Yokota, H.-O., Tsutsumi, M., Yasuda, T., Watanabe, O., Wang, S., 2005. Quantifying grazing intensities using geographic information systems and satellite remote sensing in the Xilingol steppe region, Inner Mongolia, China. *Agric. Ecosyst. Environ.* 107 (1), 83–93.

- Kiviet, J.F., 2009. Econometric analysis of panel data: editorial introduction. *Singapore Economic Review* 54 (03), 313–317. <https://doi.org/10.1142/S0217590809003355>.
- Klemas, V., 2013. Remote sensing of coastal wetland biomass: an overview. *J. Coastal Res.* 290, 1016–1028. <https://doi.org/10.2112/JCOASTRES-D-12-00237.1>.
- Li, F., Zheng, J., Wang, H., Luo, J., Zhao, Y., Zhao, R., 2016a. Mapping grazing intensity using remote sensing in the Xilingol steppe region, Inner Mongolia, China. *Remote Sensing Letters* 7 (4), 328–337. <https://doi.org/10.1080/2150704X.2015.1137987>.
- Li, Z., Guo, X., 2018. Non-photosynthetic vegetation biomass estimation in semiarid Canadian mixed grasslands using ground hyperspectral data, Landsat 8 OLI, and Sentinel-2 images. *Int. J. Remote Sens.* 39 (20), 6893–6913. <https://doi.org/10.1080/01431161.2018.1468105>.
- Li, Z., Xin, X., Tang, H., Yang, F., Chen, B., Zhang, B., 2017. Estimating grassland LAI using the random forests approach and Landsat imagery in the meadow steppe of Hulunbeier, China. *Journal of Integrative Agriculture* 16 (2), 286–297. [https://doi.org/10.1016/S2095-3119\(15\)61303-X](https://doi.org/10.1016/S2095-3119(15)61303-X).
- Li, Z., Wang, J., Tang, H., Huang, C., Yang, F., Chen, B., Wang, X., Xin, X., Ge, Y., 2016b. Predicting grassland leaf area index in the meadow steppes of northern China: a comparative study of regression approaches and hybrid geostatistical methods. *Remote Sensing* 8 (8), 632. <https://doi.org/10.3390/rs8080632>.
- Misra, G., Fiona, C., Astrid, W., 2020. Status of phenological research using Sentinel-2 data: a review. *Remote Sens.* 12 (17) <https://doi.org/10.3390/RS12172760>.
- Mohler, R.L., Douglas, G.G., 2010. A comparison of red, NIR, and NDVI for monitoring temporal burn signature change in tallgrass prairie. *Remote Sensing Letters* 1 (1), 3–9. <https://doi.org/10.1080/01431160903154291>.
- Nakagawa, S., Paul, C.D.J., Holger, S., 2017. Coefficient of determination r^2 and intra-class correlation coefficient icc from generalized linear mixed-effects models revisited and expanded. *J. R. Soc. Interface* 14 (134). <https://doi.org/10.1098/rsif.2017.0213>.
- Obermeier, W.A., Lehnert, L.W., Pohl, M.J., Makowski, G., Gianonni, S., Silva, B., Seibert, R., Laser, H., Moser, G., Müller, C., Luterbacher, J., Bendix, J., 2019. Grassland ecosystem services in a changing environment: the potential of hyperspectral monitoring. *Remote Sens. Environ.* 232, 111273. <https://doi.org/10.1016/j.rse.2019.111273>.
- Otgontbayar, M., Clement, A., Jonathan, C., Amarsaikhan, D., 2019. Mapping pasture biomass in Mongolia using partial least squares, random forest regression and Landsat 8 imagery. *Int. J. Remote Sens.* 40 (8), 3204–3226. <https://doi.org/10.1080/01431161.2018.1541110>.
- Pereira, J.M.C., 2003. Remote sensing of burned areas in tropical savannas. In: *International Journal of Wildland Fire* 12, 259–270. <https://doi.org/10.1071/wf03028>.
- Poulter, B., Frank, D., Ciais, P., Myneni, R.B., Andela, N., Bi, J., Broquet, G., Canadell, J.G., Chevallier, F., Liu, Y.Y., Running, S.W., Sitch, S., van der Werf, G.R., 2014. Contribution of semi-arid ecosystems to interannual variability of the global carbon cycle. *Nature* 509 (7502), 600–603. <https://doi.org/10.1038/nature13376>.
- Rouse, J.W., Hass, R.H., Schell, J.A., Deering, D.W., 1973. Monitoring vegetation systems in the great plains with ERTS. *Third Earth Resources Technology Satellite (ERTS) Symposium* 1, 309–317.
- Running, S.W., 1989. Mapping regional forest evapotranspiration and photosynthesis by coupling satellite data with ecosystem simulation. *Ecology* 704, 1090–1101. <https://doi.org/10.2307/1941378>.
- Schellberg, J., Verbruggen, E., 2014. Frontiers and perspectives on research strategies in grassland technology. *Crop and Pasture Science* 65 (6), 508. <https://doi.org/10.1071/CP13429>.
- Scurlock, J.M.O., Hall, D.O., 1998. The global carbon sink: a grassland perspective. *Glob. Change Biol.* 4 (2), 229–233. <https://doi.org/10.1046/j.1365-2486.1998.00151.x>.
- Sellers, P.J., Dickinson, R.E., Randall, D.A., Betts, A.K., Hall, F.G., Berry, J.A., Collatz, G.J., Denning, A.S., Mooney, H.A., Nobre, C.A., Sato, N., Field, C.B., Henderson-Sellers, A., 1997. Modeling the exchanges of energy, water, and carbon between continents and the atmosphere. *Science* 275 (5299), 502–509.
- Shoko, C., Mutanga, O., 2017. Examining the strength of the newly-launched Sentinel 2 MSI sensor in detecting and discriminating subtle differences between C3 and C4 grass species. *ISPRS J. Photogramm. Remote Sens.* 129, 32–40. <https://doi.org/10.1016/j.isprsjprs.2017.04.016>.
- Van Deventer, A.P., Ward, A.D., Gowda, P.M., Lyon, J.G., 1997. Using thematic mapper data to identify contrasting soil plains and tillage practices. *Photogramm. Eng. Remote Sens.* 63 (1), 87–93.
- Vincini, M., Amaducci, S., Frazzi, E., 2014. Empirical estimation of leaf chlorophyll density in winter wheat canopies using Sentinel-2 spectral resolution. *IEEE Trans. Geosci. Remote Sens.* 52 (6), 3220–3235.
- Wachendorf, M., Fricke, T., Möckel, T., 2018. Remote sensing as a tool to assess botanical composition, structure, quantity and quality of temperate grasslands. *Grass Forage Sci.* 73 (1), 1–14. <https://doi.org/10.1111/gfs.2018.73.issue-110.1111/gfs.12312>.
- Wang, C., Chen, J., Wu, J., Tang, Y., Shi, P., Andrew Black, T., Zhu, K., 2017. A snow-free vegetation index for improved monitoring of vegetation spring green-up date in deciduous ecosystems. *Remote Sens. Environ.* 196, 1–12. <https://doi.org/10.1016/j.rse.2017.04.031>.
- Watson, D.J., Watson, Marion.A., 1953. Comparative physiological studies on the growth of field crops : iii. the effect of infection by beet yellows and beet mosaic viruses on the growth and yield of the sugar-beet root crop. *Ann. Appl. Biol.* 40 (1), 1–37. <https://doi.org/10.1111/aab.1953.40.issue-110.1111/j.1744-7348.1953.tb02364.x>.
- Weddell, B.J., 2001. Fire in Steppe Vegetation of the Northern Intermountain Region.
- Xie, Q., Dash, J., Huete, A., Jiang, A., Yin, G., Ding, Y., Peng, D., Hall, C.C., Brown, L., Shi, Y., Ye, H., Dong, Y., Huang, W., 2019. Retrieval of crop biophysical parameters from sentinel-2 remote sensing imagery. *Int. J. Appl. Earth Obs. Geoinf.* 80, 187–195. <https://doi.org/10.1016/j.jag.2019.04.019>.
- Xie, Y., Sha, Z., Yu, M., Bai, Y., Zhang, L., 2009. A comparison of two models with Landsat data for estimating above ground grassland biomass in Inner Mongolia, China. *Ecological Modelling* 220 (15), 1810–1818.
- Xu, D., Chen, B., Yan, R., Yan, Y., Sun, X., Xu, L., Xin, X., 2019. Quantitative monitoring of grazing intensity in the temperate meadow steppe based on remote sensing data. *Int. J. Remote Sens.* 40 (5–6), 2227–2242. <https://doi.org/10.1080/01431161.2018.1500733>.
- Xu, D., Wang, C., Chen, J., Shen, M., Shen, B., Yan, R., Li, Z., Karnieli, A., Chen, J., Yan, Y., Wang, X., Chen, B., Yin, D., Xin, X., 2021. The superiority of the normalized difference phenology index (NDPI) for estimating grassland aboveground fresh biomass. *Remote Sens. Environ.* 264, 112578. <https://doi.org/10.1016/j.rse.2021.112578>.
- Yan, R., Tang, H., Xin, X., Chen, B., Murray, P.J., Yan, Y., Wang, X., Yang, G., 2016. Grazing intensity and driving factors affect soil nitrous oxide fluxes during the growing seasons in the Hulunbeier meadow steppe of China. *Environ. Res. Lett.* 11 (5), 054004. <https://doi.org/10.1088/1748-9326/11/5/054004>.
- Yan, R., Xin, X., Yan, Y., Wang, X., Zhang, B., Yang, G., Liu, S., Deng, Y., Li, L., 2015. Impacts of differing grazing rates on canopy structure and species composition in Hulunbeier meadow steppe. *Rangeland Ecol. Manage.* 68 (1), 54–64. <https://doi.org/10.1016/j.rama.2014.12.001>.
- Yu, R., Evans, A.J., Malleson, N., 2018. Quantifying grazing patterns using a new growth function based on MODIS leaf area index. *Remote Sens. Environ.* 209, 181–194. <https://doi.org/10.1016/j.rse.2018.02.034>.
- Zhang, C., Sara, D., Hannah, C., Deepak, R.M., 2018. Quantification of sawgrass marsh aboveground biomass in the coastal everglades using object-based ensemble analysis and Landsat data. *Remote Sens. Environ.* 204, 366–379. <https://doi.org/10.1016/j.rse.2017.10.018>.
- Zhu, X., Liu, D., 2015. Improving forest aboveground biomass estimation using seasonal Landsat NDVI time-series. *ISPRS J. Photogramm. Remote Sens.* 102, 222–231. <https://doi.org/10.1016/j.isprsjprs.2014.08.014>.
- Zhang, Y., Zhang, C., Wang, Z., An, R.U., Li, J., 2019. Comprehensive research on remote sensing monitoring of grassland degradation: A case study in the three-river source region, China. *Sustainability* 11 (7), 1845. <https://doi.org/10.3390/su11071845>.